communications physics

ARTICLE

https://doi.org/10.1038/s42005-023-01243-8 OPEN

Robust oscillator-mediated phase gates driven by low-intensity pulses

Iñigo Arrazola [1]✉ & Jorge Casanova [2,3,4]

Robust qubit-qubit interactions mediated by bosonic modes are central to many quantum technologies. Existing proposals combining fast oscillator-mediated gates with dynamical decoupling require strong pulses or fast control over the qubit-boson coupling. Here, we present a method based on dynamical decoupling techniques that leads to faster-than-dispersive entanglement gates with low-intensity pulses. Our method is general, i.e., it is applicable to any quantum platform that has qubits interacting with bosonic mediators via longitudinal coupling. Moreover, the protocol provides robustness to fluctuations in qubit frequencies and control fields, while also being resistant to common errors such as frequency shifts and heating in the mediator as well as crosstalk effects. We illustrate our method with an implementation for trapped ions coupled via magnetic field gradients. With detailed numerical simulations, we show that entanglement gates with infidelities of 10^{-3} or 10^{-4} are possible with current or near-future experimental setups, respectively.

[1] Vienna Center for Quantum Science and Technology, Atominstitut, TU Wien, 1040 Vienna, Austria. [2] Department of Physical Chemistry, University of the Basque Country UPV/EHU, Apartado 644, 48080 Bilbao, Spain. [3] EHU Quantum Center, University of the Basque Country UPV/EHU, Leioa, Spain. [4] IKERBASQUE, Basque Foundation for Science, Plaza Euskadi 5, 48009 Bilbao, Spain. ✉email: iarrazola003@gmail.com

High-fidelity entanglement generation among qubits is crucial for quantum information processing[1]. In most platforms, entangling gates come via direct interactions (e.g. hyperfine fields among nuclear spins) or via a bosonic mediator. Examples of the latter include solid-state qubits coupled to microwave resonators[2–6], or trapped ions sharing vibrational modes[7]. In this scenario, the paradigmatic Mølmer-Sørensen (MS) gate[8–11] and related schemes[12–14] reach entanglement operations with inherent robustness to uncertainties in the bosonic state.

In recent years, several gate schemes have been developed that operate on the same MS principle but are also robust against other sources of error[15]. Some examples are frequency or amplitude-modulated gates decoupling from mode decoherence[16–21], from spectator modes[22–28] or from deviations in the qubit-boson coupling strength[29–33]. In another vein, dynamical decoupling (DD) is a well established paradigm to protect qubits against decoherence[34,35]. Some continuous DD techniques have been demonstrated to be suitable for quantum gate implementations[36–40], while pulsed DD methods achieve increased robustness employing suited sequences such as XY8[41–48] or AXY[49–51]. However, the use of pulsed DD to protect oscillator-mediated gates has been mostly limited to dispersive regimes[52–55], and to few spin-echo[56–58] or rotary-echo[37] pulses. Note that the application of several π pulses is desirable for efficient elimination of time-varying noise.

In this regard, Manovitz et al.[59] have experimentally shown that the MS gate can be combined with pulse sequences given the ability to tune and turn on-and-off the qubit-boson coupling as many times as the number of DD pulses introduced. Another possibility explored theoretically is to combine an always-on qubit-boson coupling with strong π pulses[51,60,61]. Although this is possible in certain trapped-ion architectures, turning on-and-off the qubit-boson coupling maybe not practical in other platforms. On the other hand, the use of strong π pulses is experimentally challenging since high-power controls are needed, while these induce crosstalk and hinder the applicability in multimode scenarios.

In this article, we design a DD sequence with low-intensity π pulses—named TQXY16—that achieves faster-than-dispersive entangling gates using static (i.e. non-tunable) qubit-oscillator coupling. Importantly, our gates decouple from dephasing, pulse imperfections, and unwanted finite-pulse effects, leading to high fidelity. Furthermore, we demonstrate the versatility of our protocol by incorporating techniques that lead to additional resilience to decoherence on the bosonic mediator and potential crosstalk effects. Although our method is general, we exemplify its performance in radio-frequency controlled trapped ions demonstrating infidelities within the 10^{-3} threshold at state-of-the-art experimental conditions, and of 10^{-4} in near-future setups.

Results

Gate with instantaneous pulses. We consider a system that comprises two qubits and a bosonic mode –with frequencies ω_1, ω_2 and ν– coupled via longitudinal coupling[2–7] (here, and throughout the paper, H is $H/\hbar$, meaning all Hamiltonians are given in units of angular frequency),

$$H_0 = \nu a^\dagger a + \eta\nu(a + a^\dagger)S_z. \tag{1}$$

Here, $a^\dagger(a)$ is the creation (annihilation) operator of the bosonic mode, $S_\mu \equiv \sigma_1^\mu + \sigma_2^\mu$ with $\mu \in x, y, z$ are collective qubit operators, and $\eta\nu$ is the coupling strength. Also, note that H_0 is written in a rotating frame with respect to (w.r.t) the qubit free-energy Hamiltonian $H_q = \sum_\mu \omega_\mu \sigma_\mu^z/2$. We assume the usual experimental scenario $\eta \ll 1$, thus we stay away from other paradigms that require stronger qubit-boson couplings[62–66]. H_0 contains no driving fields, while in our method we drive the qubits for two main reasons: (i) Accelerate the gate by making the qubits rotate at a frequency close to the bosonic frequency ν, and (ii) Protection of the gate from qubit noise of the form $\epsilon_j(t)\sigma_j^z/2$ leading to dephasing. When driving the qubits, H_0 is completed with the term $H_d(t) = \sum_{\mu=x,y}\Omega_\mu(t)S_\mu/2$. In an interaction picture w.r.t. $H_d + \nu a^\dagger a$ we get

$$H(t) = \eta\nu(ae^{-i\nu t} + a^\dagger e^{i\nu t})\sum_{\mu=x,y,z} f_\mu(t)S_\mu, \tag{2}$$

where $\sum_{\mu=x,y,z} f_\mu(t)S_\mu = U_d^\dagger(t)S_z U_d(t)$ with $U_d(t) = \mathcal{T}\exp[-i\int_0^t H_d(t')dt']$ being the time-ordered propagator. See supplementary note 1 for additional details.

If driving fields are delivered as instantaneous π pulses (note this requires $\Omega_{x,y} \gg \nu$ during the application of the pulse) spaced $\tau/2$ apart, $f_{x,y}(t)$ can be neglected and $f_z(t) = 1(-1)$ if the number of applied pulses is even (odd), see the grey solid line in Fig. 1(a). For the moment we consider instantaneous pulses, while later we treat the realistic case of non-instantaneous ones. As π pulses are applied periodically, $f_z(t)$ takes the form of a function with period τ such that $f_z(t) = \sum_{n=1}^\infty f_n\cos(n\omega t)$, where $\omega = 2\pi/\tau$ and $f_n = \frac{2}{\tau}\int_0^\tau dt' f_z(t')\cos(n\omega t')$. Hence, under the assumption of instantaneous pulses we get

$$H(t) = \eta\nu\sum_{n=1}^{\infty} f_n\cos(n\omega t)(ae^{-i\nu t} + a^\dagger e^{i\nu t})S_z, \tag{3}$$

whilst setting an interpulse spacing $\tau/2 = \tau_k/2$ such that $\omega = \omega_k \approx \nu/k$ leads to a resonant qubit-boson interaction via the kth harmonic (from now on $\tau \rightarrow \tau_k$ and $\omega \rightarrow \omega_k$, where the subscript k refers to the kth harmonic). As $\eta \ll 1$, the terms in Eq. (3) that rotate with frequencies $\pm|\nu - n\omega_k|$ (where $n \neq k$) and $\pm|\nu + n\omega_k|$ can be substituted, using the rotating-wave approximation, by their second-order contribution (here, and in the rest of the paper, second-order stands for second order in η) leading to

$$H(t) \approx \frac{1}{2}\eta\nu f_k(ae^{-i\xi_k t} + \text{H.c.})S_z - \frac{1}{2}\eta^2\nu J_k S_z^2, \tag{4}$$

where $\xi_k = \nu - k\omega_k$ is the detuning w.r.t. the kth harmonic and $J_k = f_k^2/4 + \sum_{n\neq k} f_n^2/(1 - n^2/k^2)$ is an effective spin-spin coupling constant that contains contributions from all harmonics. Note that, as $\eta \ll 1$ contributions of higher order in η can be neglected. See supplementary note 2 for additional details. The propagator associated to Hamiltonian (3) is

$$U(t) = \exp\{[\alpha(t)a^\dagger - \alpha^*(t)a]S_z\} \times \exp[i\theta(t)S_z^2] \tag{5}$$

where $\alpha(t) = -i\eta\nu\int_0^t dt' f_z(t')e^{i\nu t'} \approx -\eta\nu f_k/(2\xi_k)(e^{i\xi_k t} - 1)$ and

$$\theta(t) = \text{Im}\int_C \alpha\, d\alpha \approx \frac{\eta^2\nu^2 f_k^2}{4\xi_k}\left[t - \frac{\sin(\xi_k t)}{\xi_k}\right] + \frac{1}{2}\nu\eta^2 J_k t, \tag{6}$$

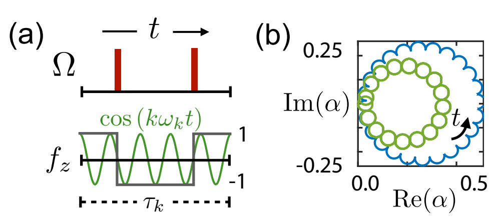

Fig. 1 Entangling gates with instantaneous π pulses. a Rabi frequency $\Omega(t)$ and modulation function $f_z(t)$ during a period τ_k for $k = 5$. For comparison, we plot $\cos(k\omega_k t)$ in green. **b** Phase-space trajectory of $\alpha(t)$ during the application of a pulse sequence with $k = 1$ and $k = 5$ in blue and green, respectively.

where $\mathcal{C}$ is the phase-space trajectory followed by $\alpha(t)$. Note that, if the gate time is chosen as $t_g = 2\pi/|\xi_k|$, $\alpha(t_g) \approx 0$ at the end of the gate, making the gate insensitive to the bosonic state. To satisfy condition $\theta(t_g) = \pi/8$, we choose τ_k such that $\xi_k = 2\eta\nu\{\sqrt{f_k^2 + 4\eta^2 J_k^2} + 2\eta J_k\}$ for $J_k > 0$. After a time t_g the propagator $U(t)$ approximates to $\exp(i\frac{\pi}{8}S_z^2)$. For two qubits, this is equivalent (up to a global qubit rotation) to the CPHASE gate, and transforms the state $|{+}{+}\rangle$ into the Bell state $|\Phi^+\rangle = \frac{1}{\sqrt{2}}(|{+}{+}\rangle + i|{-}{-}\rangle)$. It is noteworthy that the choice of ξ_k (thus τ_k) is, in general, not trivial, as both f_k and J_k depend on τ_k. However, in the cases discussed here, this dependance does not hold, making the choice of ξ_k direct. See supplementary note 3 for analytic expressions for f_k and J_k.

For instantaneous π pulses one finds $f_k = f_k^{\rm ins} = \frac{4}{k\pi}\sin(\frac{k\pi}{2})$. Thus, if resonance is achieved via a low harmonic, e.g. $k = 1$, the gate time is $t_g^{k=1} \approx \pi^2/4\eta\nu$, a factor $\pi/2$ longer than the original MS gate. On the other hand, for sufficiently large harmonics the gate is mostly governed by the dispersive term $\frac{1}{2}\eta^2\nu J_{k\to\infty} S_z^2 \approx \eta^2\nu S_z^2$ in Eq. (4), leading to $t_g^{\rm d} = \pi/8\eta^2\nu$. We define faster-than-dispersive gates as those that satisfy $t_g^k/t_g^{\rm d}<1$. For example, in the case $\eta = 0.01$ and $k = 1$ we find a faster-than-dispersive gate with $t_g^{k=1}/t_g^{\rm d} \approx 1/16$. This is, the gate is 16 times faster than the dispersive one. In Fig. 1(b), we show $\alpha(t)$ for $\eta = 0.03$, with $k = 1$ and 5.

It is noteworthy that the analysis conducted above is valid for N_q qubits homogeneously coupled to the same bosonic mode, i.e. $S_\mu \to \sum_{j=1}^{N_q} \sigma_j^\mu$. For two qubits with inhomogeneous coupling, i.e. $S_z \to S_z = (\eta_1\sigma_1^z + \eta_2\sigma_2^z)/\eta$ where $\eta_j \ll 1$, the method also yields to a CPHASE gate, however, in this case, the correct expression for the detuning ξ_k is that in which every η is substituted by $\sqrt{\eta_1\eta_2}$. For larger η, the rotating-wave approximation is not justified and terms neglected from Eq. (3) to Eq. (4) will lead to significant residual qubit-boson entanglement at the end of the gate. See supplementary note 4 for additional details.

Gate with low-intensity pulses. In what follows, we discuss the realistic case of non-instantaneous pulses. For standard top-hat pulses the Fourier coefficient f_k that quantifies the strength of the qubit-boson interaction reads (see supplementary note 3 for the derivation)

$$f_k^{\rm th} \approx \frac{f_k^{\rm ins}}{1 - \nu^2/\Omega^2}\cos\left(\frac{\pi\nu}{2\Omega}\right). \tag{7}$$

Notice that for low-intensity pulses—defined as those holding $\Omega < \nu$—the value of f_k decays with $(\Omega/\nu)^2$. As a result, achieving faster-than-dispersive gates is no longer possible. Note that f_k directly relates to the non-dispersive contribution in $\theta(t)$, and, through condition $\theta(t_g) = \pi/8$, to the gate time t_g.

To solve this problem and optimise the strength of the qubit-boson interaction, we propose to modulate the Rabi frequency during the execution of each π pulse. Specifically, we pose the following ansatz for $f_z(t)$

$$f_z(t) = \cos[\pi(t - t_i)/t_\pi] + \beta(t)\sin[k\omega_k(t - t_m)], \tag{8}$$

where t_π is the π pulse duration, and t_i and $t_m = t_i + t_\pi/2$ are the initial and central points of the pulse. Note that the Rabi frequency is then given by $\Omega(t) = -\frac{\partial f_z(t)}{\partial t} \times [1 - f_z^2(t)]^{-1/2}$. For the envelope function $\beta(t)$, we propose

$$\beta(t) = \frac{d}{\pi k b}\sin(\pi k/2)\left[\mathrm{erf}\left(\frac{t - t_l}{c t_\pi}\right) - \mathrm{erf}\left(\frac{t - t_r}{c t_\pi}\right)\right], \tag{9}$$

where $t_r = t_m + b t_\pi$ and $t_l = t_m - b t_\pi$. The free parameters b and c serve to control the width of the envelope function $\beta(t)$, while d is proportional to its amplitude. Suitable values for b, c and d for the first harmonics are shown in Table 2 (Methods).

From now on, we assume $t_\pi = \tau_k/2$, i.e., the pulse extends over a whole period $\tau_k/2$, leading to solutions with the lowest intensities. As a result of our pulse design with suitable b and c, the value for the Fourier coefficient f_k is given by $f_k^{\rm m} = -4d/\pi k$ where $|d|$ can take values from 0 to $|d_{\max}|>1$. See supplementary note 3 for the derivation. Since now f_k depends on d, this serves to control the strength of the interaction, thus the duration of the gate t_g. Also, d relates to the amplitude of the pulse, thus to the maximum value of the Rabi frequency $\Omega_{\rm pp}$. Typically, we look for large values of d, bounded by $d_{\max}$ or by the experimentally available $\Omega_{\rm pp}$.

Now we describe the recipe to design faster-than-dispersive gates using low-intensity pulses. First we choose a value for the harmonic k. Larger k allow for lower pulse intensities at the price of longer gates. Second, we use Eq. (8) to generate the modulation function $f_z(t)$ and the Rabi frequency $\Omega(t)$ for different values of d, and calculate both the gate time t_g and $\Omega_{\rm pp} = \max[|\Omega(t)|]$. We note that the obtained $\Omega(t)$ can lead to pulses along arbitrary axes (e.g. X or Y). In particular, for reasons described later, we target gates formed by concatenating blocks of 16 pulses. For that, the gate time t_g must be $8N\tau_k$, where N is an integer number. This translates into the condition $(\nu - \xi_k)/8k|\xi_k| \in \mathbb{N}$ (note $t_g = 8N\tau_k$, while $t_g = 2\pi/|\xi_k|$ and $\tau_k = 2\pi k/(\nu - \xi_k)$). The final step is to select the values of d for which this last condition is satisfied. As a result, we obtain all possible gates within the harmonic k as well as the corresponding values for $\Omega_{\rm pp}$.

Figure 2(b) shows values of t_g and $\Omega_{\rm pp}$ obtained following the previous prescription for $\eta = 0.005$ and $k = 7, 9$. Notice that there are plenty of solutions giving faster-than-dispersive gates, i.e. $t_g/t_g^{\rm d}<1$, using low-intensity pulses with values of $\Omega_{\rm pp}$ well below the frequency ν.

As an example, we choose two solutions within the 9th harmonic, where τ_k extends over approximately nine oscillator periods. In Fig. 2c the shapes of $\Omega(t)$ and $f_z(t)$ are displayed for cases $N = 5$ and 10. Notice that $\Omega(t)$ achieves a larger amplitude when $N = 5$. As a consequence, it generates a faster gate. This is shown in Fig. 2d, where the two-qubit gate phase $\theta(t)$ related to the $N = 5$ gate reaches the target value $\pi/8$ faster than the $N = 10$ gate or the dispersive gate.

The reason for choosing the gate time as an integer multiple of $8\tau_k$ has to do with an efficient decoupling from finite-pulse effects

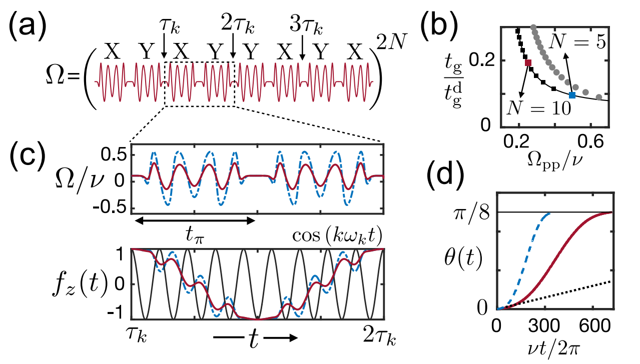

Fig. 2 Amplitude modulated π pulses. a $\Omega(t)$ for a single XY8 block. The whole sequence here is a concatenation of $2N$ blocks. **b** Gate time t_g as a function of $\Omega_{\rm pp}$, for values of d between 0 and $d_{\max}$. Values satisfying $t_g = 8N\tau_k$ are represented by square and round markers for $k = 9$ and $k = 7$, respectively. **c** $\Omega(t)$ and $f_z(t)$ for cases $N = 5$ with $d = 1.888$ (blue) and $N = 10$ with $d = 0.908$ (red) of the 9th harmonic. **d** Gate phase $\theta(t)$ for $N = 5$ (dashed blue line), $N = 10$ (solid red line), and the dispersive case (dotted line).

Table 1 Error budget: Column XY8 and TQXY16 show the infidelities after an evolution with Hamiltonians $H_d^{(+)} + H_0 + H_{2M}^{\mathrm{eff}}$ and H_s, respectively.

Gate	$\mathcal{I}_{\mathrm{XY8}}$	$\mathcal{I}_{\mathrm{TQXY16}}$	$\Delta\mathcal{I}_{\mathrm{2M}}$	$\Delta\mathcal{I}_{\mathrm{CT}}$	$\Delta\mathcal{I}_{\mathrm{CT*}}$	$\Delta\mathcal{I}_{T_2}$	$\Delta\mathcal{I}_{\delta\Omega}$	$\Delta\mathcal{I}_{\delta\nu}$	$\Delta\mathcal{I}_{\dot{n}}$	$\mathcal{I}_{\mathrm{total}}$ (10^{-4})
G1	5.50	0.01	0.04	24.8	2.26	2.34	0.21	0.28	5.65	10.8
G2	28.7	$<10^{-2}$	$<10^{-2}$	3.20	0.95	2.45	0.32	1.01	19	23.7
G3	41.3	$<10^{-2}$	$<10^{-2}$	134	1.82	2.35	0.31	0.26	4.71	9.45
G4	$>10^3$	0.12	0.38	0.23	0.01	0.43	0.09	$<10^{-2}$	0.11	1.14

The remaining columns show infidelities relative to the TQXY16 case (e.g. $\Delta\mathcal{I}_{\mathrm{2M}} = \mathcal{I}_{\mathrm{2M}} - \mathcal{I}_{\mathrm{TQXY16}}$), taking into account various experimental imperfections. In columns $\Delta\mathcal{I}_{\mathrm{2M}}$, $\Delta\mathcal{I}_{\mathrm{CT}}$, and $\Delta\mathcal{I}_{\mathrm{CT^*}}$, infidelities obtained considering a second mode, crosstalk, and crosstalk with the $\sin^2$ ramp are shown. In $\Delta\mathcal{I}_{\delta\Omega}$, $\Delta\mathcal{I}_{\delta\nu}$, and $\Delta\mathcal{I}_{T_2}$ we show relative infidelities considering static shifts of $\delta\Omega = 5\times10^{-3}$, $\delta\nu = 10^{-5}$, and $\delta\omega = (2\pi)\times 2\sqrt{2}$ kHz. $\dot{n}$ shows the error considering heating with rates $\dot{n}_1 = 35$ ph/s and $\dot{n}_2 = 100$ ph/s for regimes (i) and (ii), respectively. The last column shows the overall error obtained by summing the values of all columns except those in $\mathcal{I}_{\mathrm{XY8}}$ and $\Delta\mathcal{I}_{\mathrm{CT}}$.

produced by the terms $f_{x,y}(t)$ neglected in Eq. (3). In the same way, the XY8 ≡ XYXYYXYX pulse structure assures cancelation of σ^z type noise, as well as of Rabi frequency fluctuations. In Fig. 2a the Rabi frequency is plotted ($\Omega_x(t)$ when 'X'; $\Omega_y(t)$ when 'Y') for an XY8 block.

To understand the elimination of finite-pulse effects, we calculate the second-order Hamiltonian of Eq. (2) after an XYXY block leading to (see supplementary note 5 for the derivation)

$$H_{\mathrm{XYXY}} = -\frac{1}{2}\eta^2\nu\left\{J_k^{\perp}(S_x^2+S_y^2) - B_k(a^\dagger a)S_z\right\}. \qquad (10)$$

If our gate contains only XYXY blocks, H_{XYXY} adds to Hamiltonian (4) spoiling a high-fidelity performance. To overcome this problem, we use a two-step strategy. Firstly, we concatenate XYXY and YXYX blocks (which form a XY8 block) such that the term $B_k(a^\dagger a)S_z$ gets refocused. Note that in the presence of bosonic decoherence, this term will induce qubit dephasing. Secondly, we cancel the remaining term $J_k^{\perp}(S_x^2+S_y^2)$ by driving the two qubits with opposite phases every second XY8 block. This is, when rotating by an angle π the phase of the second qubit's driving $H_d^{(+)} = \sum_{\mu=x,y}\Omega_\mu(t)S_\mu^{(+)}/2$ becomes $H_d^{(-)} = \sum_{\mu=x,y}\Omega_\mu(t)S_\mu^{(-)}/2$ instead, where $S_\mu^{(\pm)} \equiv \sigma_1^\mu \pm \sigma_2^\mu$. This changes the sign of the $\sigma_1^u\sigma_2^\mu$ terms with $u,\mu \in \{x,y\}$, leading to refocusing of the term $J_k^{\perp}(S_x^2+S_y^2)$ after every pair of XY8 blocks.

Note that the second step requires the ability to address each qubit individually, and assumes that $N_q = 2$, i.e. S_μ is given by the sum of two qubit operators. In the absence of individual addressing, one can incorporate the term $J_k^{\perp}(S_x^2+S_y^2)$ into the gate, but then the operation applied is not equivalent to the CPHASE gate. For a discussion regarding this alternative gate, as well as the extension to the multiqubit case, see supplementary note 6.

Summarising, our two-qubit gates are generated by nesting TQXY16 ≡ XY8$^{(+)}$XY8$^{(-)}$ blocks, where TQXY16 stands for 'two-qubit' XY16, while XY8$^{(\pm)}$ implies qubits driven in phase or in anti-phase as discussed in the previous paragraph, while, importantly, each π pulse is implemented according to the designs for $f_z(t)$ and $\beta(t)$ presented in Eqs. (8), (9).

Trapped-ion implementation and numerical results. We benchmark our method by simulating its performance in a pair of trapped ions in a static magnetic field gradient[7]. In this scenario, qubit frequencies ω_μ take values around $(2\pi)\times 10$ GHz, $\nu = (2\pi)\times 220$ kHz is the frequency of the centre-of-mass vibrational mode, $\eta = \gamma_e g_B/8\nu\sqrt{\hbar/M\nu}$ is an effective Lamb-Dicke factor where $\gamma_e = (2\pi)\times 2.8$ MHz/G, g_B is the magnetic field gradient, and M is the ion mass. The two-ion system has a second vibrational mode 'b' with its corresponding qubit-boson coupling. Thus, Hamiltonian (1) is replaced by $H_0 + H_{2\mathrm{M}}$, where $H_{2\mathrm{M}} = \sqrt{3}\nu b^\dagger b - 3^{-1/4}\eta\nu(b+b^\dagger)S_z^{(-)}$. The addition of $H_{2\mathrm{M}}$ changes the dispersive coupling in Eq. (4) as $J_k \to J_k - 1/3\sum_{n=1}^{\infty} f_n^2/(1-n^2/3k^2)$, which must be taken into account when following the prescription to calculate the valid gates. This step can be done for an arbitrary amount of spectator modes, given that the mode frequencies ν_m fulfil the condition $\eta f_n \ll |\nu_m - n\omega_k|$ for all odd n.

Although we simulate the performance of the gate with the two-mode Hamiltonian $H_f = H_d^{(\pm)} + H_0 + H_{2\mathrm{M}}$ (see column $\Delta\mathcal{I}_{2M}$ in Table 1), due to computational limitations we use the single-mode Hamiltonian $H_s = H_d^{(\pm)} + H_0 + H_{2\mathrm{M}}^{\mathrm{eff}}$ instead, where $H_{2\mathrm{M}}^{\mathrm{eff}} = \frac{1}{3}\nu\eta^2 r S_z^2$ is the second-order contribution of $H_{2\mathrm{M}}$. See supplementary note 7 for additional details. Here, $H_d^{(\pm)}$ stands for $H_d^{(+)}$ ($H_d^{(-)}$) every first (second) half of a TQXY16 block.

We investigate two regimes: (i) $\eta = 0.005$ ($g_B = 19.16\ T/m$), which is the state-of-the-art of current experiments[18,54], and (ii) $\eta = 0.04$ ($g_B = 153.2$ T/m), which can be reached in near future setups[39].

In regime (i), we consider three different gates, all within the 9th harmonic. The first gate (G1), with a duration $t_g = 1.64$ ms, appears after five TQXY16 blocks with pulse length $t_\pi = 20.5$ μs reaching $\Omega_{\mathrm{pp}} = (2\pi)\times 124$ kHz. The second gate (G2) with gate time $t_g = 3.28$ ms uses ten TQXY16 blocks with pulse length $t_\pi = 20.5$ μs reaching $\Omega_{\mathrm{pp}} = (2\pi)\times 77.8$ kHz. The third gate (G3), with the gate-time $t_g = 3.94$ ms and $\Omega_{\mathrm{pp}} = (2\pi)\times 78.69$ kHz, uses twelve blocks, each with a different pulse length and detuning, while it incorporates a technique to mitigate errors due to mode decoherence, see supplementary note 8. In regime (ii) we consider a gate within the 5th harmonic (G4). This gate occurs after two TQXY16 blocks where $t_g = 368$ μs, $t_\pi = 11.5$ μs, and $\Omega_{\mathrm{pp}} = (2\pi)\times 80.9$ kHz. For further details regarding pulse parameters, see supplementary note 7.

The performance of the four gates in the presence of distinct error sources is shown in Table 1. Each simulated experiment starts from the state $|+_x+_y\rangle$ and targets the Bell-state $|\tilde{\Phi}^+\rangle = \frac{1}{\sqrt{2}}(|+_x+_y\rangle + i|-_x-_y\rangle)$, while in all cases we consider an initial motional thermal state with $\bar{n} = 1$[54]. Other initial states result in similar values for fidelity.

In the 2nd and 3rd columns of Table 1, we show the gate error $\mathcal{I} = 1 - \mathcal{F}$ obtained by concatenating XY8 or TQXY16 blocks, respectively. Here, $\mathcal{F} = \langle\tilde{\Phi}^+|\rho|\tilde{\Phi}^+\rangle/\sqrt{\mathrm{Tr}(\rho^2)}$[67], where ρ is the final state after tracing out the bosonic states. Notice that TQXY16 blocks achieve a clearly superior performance due to efficient decoupling from finite pulse effects. For these, $\mathcal{I}_{\mathrm{TQXY16}} \le 10^{-6}$ for all gates except G4, where finite the residual qubit-boson entanglement limits the error to approximately 10^{-5}. In the fourth column we evaluate the effect of the second mode b by numerically simulating the two-mode Hamiltonian H_f (initialising the second mode b in a thermal state with $\bar{n} = 1$), which results in $\mathcal{I}_{2\mathrm{M}}$. The infidelities relative to the previous case

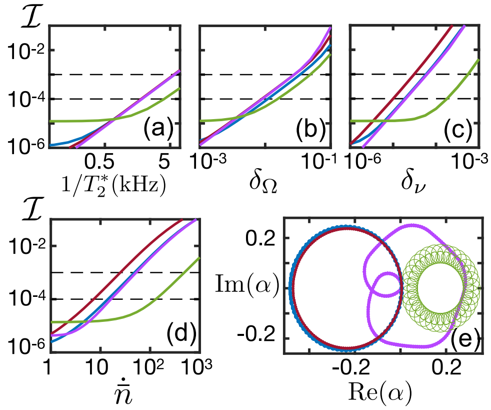

Fig. 3 Sensitivity to errors. a Gate error $\mathcal{I}$ versus $1/T_2^*$ for the gates G1 (blue), G2 (red), G3 (purple) and G4 (green). In (**b**) and (**c**), the error is shown for Rabi frequency shifts $\Omega(t) \to (1 \pm \delta_\Omega)\Omega(t)$ and in the mode frequency $\nu \to (1 \pm \delta_\nu)\nu$. **d** Error under heating for different rates $\dot{\bar{n}}$. **e** Trajectory of $\alpha(t)$ for gates G1 (circular, blue), G2 (circular, red), G3 (non-circular, purple), and G4 (circular, green).

(i.e. $\Delta\mathcal{I}_{2M} = \mathcal{I}_{2M} - \mathcal{I}_{TQXY16}$) are given in the '$\Delta\mathcal{I}_{2M}$' column of Table 1. Again, the effect of the second mode is relevant only for G4, which contributes 3.8×10^{-5} to the total error. Importantly, this demonstrates that our gate is compatible with the presence of spectator modes.

To investigate the effect of crosstalk, we add the term $H_c^{(\pm)} = \sum_{\mu=x,y} \frac{\Omega_\mu(t)}{2}(\sigma_2^- e^{-i\Delta\omega t} \pm \sigma_1^- e^{i\Delta\omega t} + \mathrm{H.c.})$ to H_s, where $\Delta\omega/(2\pi) = (\omega_2 - \omega_1)/(2\pi) = 2.54$ and 20.34 MHz for regimes (i) and (ii), respectively. The results are given in the '$\Delta\mathcal{I}_{CT}$' column of Table 1. In contrast to the effect of the spectator mode, crosstalk is most harmless with the G4 gate. This is expected, as G4 operates with a larger qubit detuning $\Delta\omega$ than the rest, while using a similar Rabi frequency. To reduce the impact of crosstalk, we combine our pulses with $\sin^2$-shaped ramps at the beginning and end of each pulse, see supplementary note 7, and optimise the length of the ramp using numerical simulations. The resulting infidelities are shown in the '$\Delta\mathcal{I}_{CT*}$' column. Note that the $\sin^2$ ramp reduces the value of $\mathcal{I}$ by at least an order of magnitude in most cases.

Robustness w.r.t. common errors such as dephasing over qubits due to static shifts $\omega_j \to \omega_j \pm \delta\omega$, Rabi-frequency shifts (i.e. $\Omega(t) \to (1 \pm \delta_\Omega)\,\Omega(t)$), and shifts on the mode frequency, $\nu \to (1 \pm \delta_\nu)\,\nu$, is shown in Fig. 3a–c, where the infidelity is plotted versus the degree of uncertainty. In columns 7–9 of Table 1, we display the relative infidelities for a dephasing time $T_2^* \approx 500\mu s$ [54], a Rabi-frequency shift $\delta_\Omega = 5 \times 10^{-3}$, and a mode-frequency shift of $\delta_\nu = 10^{-5}$[68]. For further details, see 'Methods'. Furthermore, in Fig. 3d we plot the infidelity versus $\dot{\bar{n}}$, while in column $\dot{\bar{n}}$, we show the relative infidelities for G1-3 and G4 for mode heating rates $\dot{\bar{n}} = 35$ and 100 ph/s, respectively. For further details, see Supplementary note 7. Figure 3e shows the phase-space trajectory of $\alpha(t)$ for all gates G1-4.

Table 1 shows that mode heating is the main source of error for gates in regime (i). This, along with dephasing and crosstalk, limits the fidelity of these gates to the 10^{-3} regime. Despite its longer gate duration, G3 achieves better performance in terms of motion-induced errors than G1 and G2, proving the validity of the mode decoherence protecting technique described in supplementary note 8. Finally, table 1 shows that G4 is the most robust w.r.t. experimental imperfections. This is reasonable since it uses a larger η and is an order of magnitude faster than the other gates. In particular, we find that G4 achieves infidelities on the 10^{-4} regime, mainly limited by residual qubit-boson entanglement caused by off-resonant harmonics and the spectator mode. Note that the influence of this error has been taken into account in supplementary note 3, where we also discuss the potential effects of micromotion.

Table 2 Suitable pulse parameters.

k	3	5	7	9	11	13	15
b	0.33	0.30	0.29	0.33	0.34	0.35	0.30
c	0.035	0.04	0.05	0.042	0.03	0.035	0.035
d_{max}	−2.3	−1.5	2.4	2.3	1.9	1.7	2.3

Suitable values for b, c and $|d_{max}|$. $|d_{max}|$ corresponds to the maximum value of $|d|$ for which a physical pulse (i.e, $|f_z|(t) \le 1$) can still be generated.

Discussion

We have presented a DD sequence (TQXY16) based on the delivery of low-intensity π pulses that achieve faster-than-dispersive two-qubit gates. Without the need of any numerical optimisation, we have designed entangling gates which are robust to fluctuations in qubit frequencies and control fields, as well as to finite-pulse effects hindering a high-fidelity performance. In addition, we have demonstrated the versatility of our protocol to adopt forms that provide increased robustness against crosstalk and mode decoherence.

Our scheme is best suited for systems i) using longitudinal qubit-boson coupling with $\eta \ll 1$, ii) where dephasing is the main source of qubit decoherence, and iii) where the Rabi frequencies $\Omega(t)$ are of the order (or far below) the mode frequencies ν. This is the case, e.g., for spin qubits coupled to microwave cavities[5,6]. In ref. [6], $\eta \sim 10^{-2}$ and $\Omega/\nu \sim 0.1$. Superconducting qubit architectures exploiting longitudinal qubit-boson coupling has also been proposed[3,4]. Our method is also well suited for these systems when working with small η.

Finally, we tested the performance of our protocol in trapped ions coupled via static magnetic field gradients, where conditions (i), (ii), and (iii) are perfectly satisfied. Compared to existing multi-level schemes[18,39], our method has the advantage of using only two levels, which lowers the experimental requirements. Compared to previous pulsed DD methods[51], our method has the advantage of using realistic pulse intensities. Using detailed numerical simulations, we have obtained infidelities within the 10^{-3} threshold at state-of-the-art conditions, and in the 10^{-4} regime in near-future setups.

Methods

In Table 2 we show suitable values of b and c given the harmonic k. Also, we show the maximum value of $|d|$ for which a physical pulse (i.e, $|f_z|(t) \le 1$) can still be generated with the ansatz given in Eqs. (8), (9). For gates G1, G2 and G4, the selected values of d are 1.915, 0.933, and −0.321, respectively. The list of detunings used in gate G3 is $\vec{\xi}_k = (2\pi) \times [1.24, 0.31, 0.64, 0.09, 0.55, 0.05, 0.54, 0.06, 0.57, 0.14, 0.73, 0.80]$ kHz.

Our numerical simulations for dephasing consider an additional $\pm\,\delta\omega/2S_z$ term in H_s, where $\delta\omega = \sqrt{2}/T_2^*$. In all three cases, each point is the average error obtained by a positive (e.g. $\omega_j \to \omega_j + \delta\omega$) and a negative (e.g. $\omega_j \to \omega_j - \delta\omega$) displacement.

Data availability

Data sharing not applicable to this article as no datasets were generated or analysed during the current study.

Received: 9 December 2022; Accepted: 19 May 2023;
Published online: 29 May 2023

References

1. Nielsen, M. A. & Chuang, I. L. *Quantum Computation and Quantum Information* (Cambridge University Press, Cambridge, 2000).

2. Jin, P.-Q., Marthaler, M., Shnirman, A. & Schön, G. Strong coupling of spin qubits to a transmission line resonator. *Phys. Rev. Lett.* **108**, 190506 (2012).
3. Billangeon, P.-M., Tsai, J. S. & Nakamura, Y. Circuit-QED-based scalable architectures for quantum information processing with superconducting qubits. *Phys. Rev. B* **91**, 094517 (2015).
4. Richer, S. & DiVincenzo, D. Circuit design implementing longitudinal coupling: a scalable scheme for superconducting qubits. *Phys. Rev. B* **93**, 134501 (2016).
5. Beaudoin, F., Lachance-Quirion, D., Coish, W. A. & Pioro-Ladrière, M. Coupling a single electron spin to a microwave resonator: controlling transverse and longitudinal couplings. *Nanotechnology* **27**, 464003 (2016).
6. Bosco, S., Scarlino, P., Klinovaja, J. & Loss, D. Fully tunable longitudinal spin-photon interactions in Si and Ge quantum dots. *Phys. Rev. Lett.* **129**, 066801 (2022).
7. Mintert, F. & Wunderlich, C. Ion-trap quantum logic using long-wavelength radiation. *Phys. Rev. Lett.* **87**, 257904 (2001).
8. Sørensen, A. & Mølmer, K. Quantum computation with ions in thermal motion. *Phys. Rev. Lett.* **82**, 1971 (1999).
9. Solano, E., de Matos Filho, R. L. & Zagury, N. Deterministic Bell states and measurement of the motional state of two trapped ions. *Phys. Rev. A* **59**, R2539(R) (1999).
10. Sørensen, A. & Mølmer, K. Entanglement and quantum computation with ions in thermal motion. *Phys. Rev. A* **62**, 022311 (2000).
11. Sackett, C. A. et al. Experimental entanglement of four particles. *Nature* **404**, 256 (2000).
12. Milburn, G. J., Schneider, S. & James, D. F. V. Ion trap quantum computing with warm ions. *Fortschr. Phys.* **48**, 801 (2000).
13. Leibfried, D. et al. Experimental demonstration of a robust, high-fidelity geometric two ion-qubit phase gate. *Nature* **422**, 412 (2003).
14. Zheng, S.-B. Unconventional geometric quantum phase gates with a cavity QED system. *Phys. Rev. A* **70**, 052320 (2004).
15. Valahu, C. H., Apostolatos, I., Weidt, S. & Hensinger, W. K. Quantum control methods for robust entanglement of trapped ions. *J. Phys. B: At. Mol. Opt. Phys.* **55**, 204003 (2022).
16. Cross, A. W. & Gambetta, J. M. Optimized pulse shapes for a resonator-induced phase gate. *Phys. Rev. A* **91**, 032325 (2015).
17. Haddadfarshi, F. & Mintert, F. High fidelity quantum gates of trapped ions in the presence of motional heating. *New J. Phys.* **18**, 123007 (2016).
18. Webb, A. E. et al. Resilient entangling gates for trapped ions. *Phys. Rev. Lett.* **121**, 180501 (2018).
19. Shapira, Y., Shaniv, R., Manovitz, T., Akerman, N. & Ozeri, R. Robust entanglement gates for trapped-ion qubits. *Phys. Rev. Lett.* **121**, 180502 (2018).
20. Zarantonello, G. et al. Robust and resource-efficient microwave near-field entangling $^{9}Be^{+}$ gate. *Phys. Rev. Lett.* **123**, 260503 (2019).
21. Sutherland, R. T. et al. Laser-free trapped-ion entangling gates with simultaneous insensitivity to qubit and motional decoherence. *Phys. Rev. A* **101**, 042334 (2020).
22. Hayes, D. et al. Coherent error suppression in multiqubit entangling gates. *Phys. Rev. Lett.* **109**, 020503 (2012).
23. Choi, T. et al. Optimal quantum control of multimode couplings between trapped ion qubits for scalable entanglement. *Phys. Rev. Lett.* **112**, 190502 (2014).
24. Green, T. J. & Biercuk, M. J. Phase-modulated decoupling and error suppression in qubit-oscillator systems. *Phys. Rev. Lett.* **114**, 120502 (2015).
25. Leung, P. H. et al. Robust 2-qubit gates in a linear ion crystal using a frequency-modulated driving force. *Phys. Rev. Lett.* **120**, 020501 (2018).
26. Schäfer, V. M. et al. Fast quantum logic gates with trapped-ion qubits. *Nature* **555**, 75 (2018).
27. Lu, Y. et al. Global entangling gates on arbitrary ion qubits. *Nature* **572**, 363 (2019).
28. Milne, A. R. et al. Phase-modulated entangling gates robust to static and time-varying errors. *Phys. Rev. Applied* **13**, 024022 (2020).
29. Puri, S. & Blais, A. High-fidelity resonator-induced phase gate with single-mode squeezing. *Phys. Rev. Lett.* **116**, 180501 (2016).
30. Royer, B., Grimsmo, A. L., Didier, N. & Blais, A. Fast and high-fidelity entangling gate through parametrically modulated longitudinal coupling. *Quantum* **1**, 11 (2017).
31. Ge, W. et al. Trapped ion quantum information processing with squeezed phonons. *Phys. Rev. Lett.* **122**, 030501 (2019).
32. Burd, S. C. et al. Quantum amplification of boson-mediated interactions. *Nat. Phys.,* **17**, 898 (2021).
33. Shapira, Y., Cohen, S., Akerman, N., Stern, A. & Ozeri, R. Robust two-qubit gates for trapped ions using spin-dependent squeezing. *Phys. Rev. Lett.* **130**, 030602 (2023).
34. Viola, L. & Lloyd, S. Dynamical suppression of decoherence in two-state quantum systems. *Phys. Rev. A* **58**, 2733 (1998).
35. Ban, M. Photon-echo technique for reducing the decoherence of a quantum bit. *J. Mod. Opt.* **45**, 2315 (1998).
36. Timoney, N. et al. Quantum gates and memory using microwave-dressed states. *Nature* **476**, 185 (2011).
37. Tan, T. R. et al. Demonstration of a dressed-state phase gate for trapped ions. *Phys. Rev. Lett.* **110**, 263002 (2013).
38. Harty, T. P. et al. High-fidelity trapped-ion quantum logic using near-field microwaves. *Phys. Rev. Lett.* **117**, 140501 (2016).
39. Weidt, S. et al. Trapped-ion quantum logic with global radiation fields. *Phys. Rev. Lett.* **117**, 220501 (2016).
40. Guo, Q. et al. Dephasing-insensitive quantum information storage and processing with superconducting qubits. *Phys. Rev. Lett.* **121**, 130501 (2018).
41. Carr, H. Y. & Purcell, E. M. Effects of diffusion on free precession in nuclear magnetic resonance experiments. *Phys. Rev.* **94**, 630 (1954).
42. Meiboom, S. & Gill, D. Modified spin-echo method for measuring nuclear relaxation times. *Rev. Sci. Instrum.* **29**, 688 (1958).
43. Gullion, T., Baker, D. B. & Conradi, M. S. New, compensated carr-purcell sequences. *J. Magn. Reson. (1969)* **89**, 479 (1990).
44. Souza, A. M., Álvarez, G. A. & Suter, D. Robust dynamical decoupling. *Phil. Trans. R. Soc. A.* **370**, 4748 (2012).
45. Kabytayev, C. et al. Robustness of composite pulses to time-dependent control noise. *Phys. Rev. A* **90**, 012316 (2014).
46. Munuera-Javaloy, C., Arrazola, I., Solano, E. & Casanova, J. Double quantum magnetometry at large static magnetic fields. *Phys. Rev. B* **101**, 104411 (2020).
47. Dong, L., Arrazola, I., Chen, X. & Casanova, J. Phase-adaptive dynamical decoupling methods for robust spin-spin dynamics in trapped ions. *Phys. Rev. Applied* **15**, 034055 (2021).
48. Ezzell, N., Pokharel, B., Tewala, L., Quiroz, G. & Lidar, D.A. Dynamical decoupling for superconducting qubits: a performance survey. https://arxiv.org/abs/2207.03670 *arXiv:2207.03670* (2022).
49. Casanova, J., Wang, Z.-Y., Haase, J. F. & Plenio, M. B. Robust dynamical decoupling sequences for individual-nuclear-spin addressing. *Phys. Rev. A* **92**, 042304 (2015).
50. Casanova, J., Wang, Z.-Y. & Plenio, M. B. Arbitrary nuclear-spin gates in diamond mediated by a nitrogen-vacancy-center electron spin. *Phys. Rev. A* **96**, 032314 (2017).
51. Arrazola, I. et al. Pulsed dynamical decoupling for fast and robust two-qubit gates on trapped ions. *Phys. Rev. A* **97**, 052312 (2018).
52. Piltz, C., Scharfenberger, B., Khromova, A., Varón, A. F. & Wunderlich, C. Protecting conditional quantum gates by robust dynamical decoupling. *Phys. Rev. Lett.* **110**, 200501 (2013).
53. Qiu, J. et al. Suppressing coherent two-qubit errors via dynamical decoupling. *Phys. Rev. Applied* **16**, 054047 (2021).
54. Barthel, P. et al. Robust Two-qubit gates using pulsed dynamical decoupling, *New J. Phys.* https://doi.org/10.1088/1367-2630/acd4db (2023).
55. Morong, W. et al. Engineering dynamically decoupled quantum simulations with trapped ions. *PRX Quantum* **4**, 010334 (2023).
56. Paik, H. et al. Experimental demonstration of a resonator-induced phase gate in a multiqubit circuit-QED system. *Phys. Rev. Lett.* **117**, 250502 (2016).
57. Ballance, C. J., Harty, T. P., Linke, N. M., Sepiol, M. A. & Lucas, D. M. High-fidelity quantum logic gates using trapped-ion hyperfine qubits. *Phys. Rev. Lett.* **117**, 060504 (2016).
58. Băzăvan, O. et al. Synthesizing a $\hat{\sigma}_z$ spin-dependent force for optical, metastable, and ground state trapped-ion qubits. *Phys. Rev. A* **107**, 022617 (2023).
59. Manovitz, T. et al. Fast dynamical decoupling of the mølmer-sørensen entangling gate. *Phys. Rev. Lett.* **119**, 220505 (2017).
60. Rabl, P. et al. A quantum spin transducer based on nanoelectromechanical resonator arrays. *Nat. Phys.* **6**, 602 (2010).
61. Rosenfeld, E., Riedinger, R., Gieseler, J., Schuetz, M. & Lukin, M. D. Efficient entanglement of spin qubits mediated by a hot mechanical oscillator. *Phys. Rev. Lett.* **126**, 250505 (2021).
62. García-Ripoll, J. J., Zoller, P. & Cirac, J. I. Speed optimized two-qubit gates with laser coherent control techniques for ion trap quantum computing. *Phys. Rev. Lett.* **91**, 157901 (2003).
63. Duan, L.-M. Scaling ion trap quantum computation through fast quantum gates. *Phys. Rev. Lett.* **93**, 100502 (2004).
64. Steane, A. M., Imreh, G., Home, J. P. & Leibfried, D. Pulsed force sequences for fast phase-insensitive quantum gates in trapped ions. *New J. Phys.* **16**, 053049 (2014).
65. Bentley, C. D. B., Carvalho, A. R. R., Kielpinski, D. & Hope, J. J. Fast gates for ion traps by splitting laser pulses. *New J. Phys.* **15**, 043006 (2013).
66. Sameti, M., Lishman, J. & Mintert, F. Strong-coupling quantum logic of trapped ions. *Phys. Rev. A* **103**, 052603 (2021).
67. Wang, X., Yu, C.-S. & Yi, X. An alternative quantum fidelity for mixed states of qubits. *Phys. Lett. A* **373**, 58 (2008).
68. Johnson, K. G. et al. Active stabilization of ion trap radiofrequency potentials. *Rev. Sci. Instrum.* **87**, 053110 (2016).

Acknowledgements

I.A. would like to thank P. Rabl and J. S. Pedernales for useful discussions. I.A. acknowledges support from the European Union's Horizon2020 research and innovation programme under Grant Agreement No. 899354 (SuperQuLAN). J. C. acknowledges the Ramón y Cajal (RYC2018-025197-I) research fellowship, the financial support from Spanish Government via EUR2020-112117 and Nanoscale NMR and complex systems (PID2021-126694NB-C21) projects, the EU FET Open Grant Quromorphic (828826), the ELKARTEK project Dispositivos en Tecnologías Cuánticas (KK-2022/00062), and the Basque Government grant IT1470-22.

Author contributions

I.A. and J.C. conceived the idea. I.A. performed all the calculations. I.A. and J.C. wrote the manuscript.

Competing interests

The authors declare no competing interests.

Additional information

Supplementary information The online version contains supplementary material available at https://doi.org/10.1038/s42005-023-01243-8.

Correspondence and requests for materials should be addressed to Iñigo Arrazola.

Peer review information *Communications Physics* thanks Ralf Riedinger and the other, anonymous, reviewer(s) for their contribution to the peer review of this work.